Preparation, Sintering, and Electrochemical Properties of Tin Dioxide and Al-Doped Tin Dioxides Obtained from Citrate Precursors

R. Alcántara,[†,§] F. J. Fernández-Madrigal,[†] C. Pérez-Vicente,[†] J. L. Tirado,*[,†] Jean Claude Jumas,[‡] and Josette Olivier-Fourcade[‡]

Laboratorio de Química Inorgánica, Universidad de Córdoba, Campus de Rabanales, Edificio C3, planta 1, 14071 Córdoba, Spain, and Laboratoire de Physicochimie de la Matière Condensée (UMR 5617 CNRS), Place Eugène Bataillon, 34095 Montpellier Cedex 5, France

Received November 19, 1999. Revised Manuscript Received July 24, 2000

The metal−citrate method is applied to the preparation of microcrystalline tin dioxide and aluminum-doped materials. The effect of the precursor composition, referred to as the metal/citrate ratio, and the thermal treatment are discussed. The different compositions produce upon thermal decomposition rutile-type SnO_2 solids. For Al-containing oxide materials, Al(III) ions occupy octahedral sites isomorphic to Sn(IV), as shown by ^{27}Al MAS NMR signals at ≈0 ppm and ^{119}Sn Mössbauer signals at 0 mm/s isomer shift and 0.53 mm/s quadrupole splitting, respectively. A large microstrain content is released by successive thermal treatments at 450 °C. Simultaneously, extended defects, which imply deviations from an MO_2 stoichiometry, are found upon heating. These phenomena condition the ability of the oxide products to be used as the active anode material in lithium-ion batteries. The best electrochemical performance of lithium anode cells is achieved for 10% Al-containing ex biscitrate oxides in which ≈200 Ah/kg capacities are obtained after 30 cycles.

Introduction

In the field of promising materials for the negative electrode of lithium-ion cells, a recent advance was achieved by the introduction of tin-containing glasses by members of the Fuji research laboratories in 1997.[1] Since then, a great effort has been devoted to examining the aptitude of different tin-containing compounds as the active electrode in lithium batteries. Among the solids studied so far are crystalline and disordered oxides such as SnO, Li_2SnO_3, and SnO_2.[2−4]

On the other hand, semiconducting tin dioxide films and ceramics are widely used as gas sensors. The conductivity of the oxide can be improved by doping with other elements such as Sb,[5] which allows its use as stable electrodes for glass-melting furnaces. Besides, Cu(II) doping improves the sintering ability.[6] In the preparation of pure tin dioxide and doped derivatives, several routes have been developed depending on the application to be given: for the preparation of coatings and films, spray pyrolysis,[7] sol−gel,[5] and dip-coating[8] procedures have been reported. For the powdered material, the sol−gel route using inorganic hydrosols[6,9] and tin alkoxides[10] has been used. The major drawbacks associated with the latter procedure are the high cost of the alkoxides and their marked sensitivity to air and moisture.

The preparation of lithium−transition metal oxides for the positive electrode of advanced lithium batteries has been reported by the low-temperature decomposition of precursor solids containing the citrate chelating agent. Thus, $LiMn_2O_4$,[11] $LiCoO_2$,[12] and $LiNiO_2$[13] precursor citrates have been prepared by ethanol dehydration of citrate salts in aqueous solutions. The precursor route allows the synthesis of nanocrystals of the mixed oxides, with good control over the composition and structure as well as improved electrochemical behavior, as compared with other conventional preparative procedures. Recently, Deacon et al.[14] prepared a tin(II) citrate of $Sn_2(C_6H_8O_7)$ stoichiometry and related monotin salts of alkyl citrates with other cations such as Na^+, K^+, NH_4^+, and NR_4^+.

* To whom correspondence should be addressed.
† Universidad de Córdoba.
‡ Laboratoire de Physicochimie de la Matière Condensée.
§ Present address: SAFT, Direction de la Recherche, 111 Boulevard Alfred Daney, 33074 Bordeaux, France.

(1) Idota, Y.; Kubota, T.; Matsufuji, A.; Maekawa, Y.; Miyasaka, T. *Science* **1997**, *276*, 1395.
(2) Courtney, A.; Dahn, J. R. *J. Electrochem. Soc.* **1997**, *144*, 2045.
(3) Liu, W.; Huang, X.; Wang, Z.; Li, H.; Chen, L. *J. Electrochem. Soc.* **1997**, *145*, 59.
(4) Courtney, I. A.; Dahn, J. R. *J. Electrochem. Soc.* **1997**, *144*, 2943.
(5) Orel, B.; Lavrencic-Stangar, U.; Crnjak-Orel, Z.; Bukovec, P.; Kosec, M. *J. Non-Cryst. Solids* **1994**, *167*, 272.
(6) Santilli, C. V.; Pulcinelli, S. H.; Brito, G. E. S.; Briois, V. *J. Phys. Chem. B* **1999**, *103*, 2660.
(7) Arai, T. *J. Phys. Soc. Jpn.* **1960**, *15*, 916.
(8) Takahashi, Y.; Wada, Y. *J. Electrochem. Soc.* **1990**, *137*, 267.
(9) Davis, S. R.; Chadwick, A. V.; Wright, J. D. *J. Mater. Chem.* **1998**, *8*, 2065.
(10) Mehrota, R. C. *J. Non-Cryst. Solids* **1990**, *121*, 1.
(11) Choy, J. H.; Kim, D. H.; Kwon, C. W.; Hwang, S. J.; Kim, Y. I. *J. Power Sources* **1999**, *77*, 1.
(12) Zhecheva, E.; Stoyanova, R.; Gorova, M.; Alcantara, R.; Morales, J.; Tirado, J. L. *Chem. Mater.* **1996**, *8*, 1429.
(13) Alcántara, R.; Lavela, P.; Tirado, J. L.; Stoyanova, R.; Kuzmanova, E.; Zhecheva, E. *Chem. Mater.* **1997**, *9*, 2145.
(14) Deacon, P. R.; Mahon, M. F.; Molloy, K. C.; Waterfield, P. C. *J. Chem. Soc., Dalton Trans.* **1997**, 3705.

10.1021/cm991180i CCC: $19.00 © 2000 American Chemical Society
Published on Web 09/15/2000

The aim of this study is to evaluate the performance of the citrate method for the preparation of SnO_2. From the viewpoint of its application, the expected advantages are the low cost of the reagents, the low temperature required for the thermal decomposition of the precursors, and the ultrafine nature of the particles obtained. The possible introduction of other elements is evaluated for the aluminum case. In an attempt to monitor the nature of the precursors, FTIR spectroscopy is used. To obtain detailed information about the local environment of tin and bonding in the Sn-containing products, ^{119}Sn Mössbauer spectroscopy and X-ray absorption are used. Finally, the electrochemical performance of the oxide products is evaluated in lithium cells.

Experimental Section

For the preparation of undoped (and doped) tin citrate solutions, the amount of citric acid corresponding to the desired stoichiometry of the solid precursor was dissolved in the minimum amount of distilled water. The pH was then adjusted to 7 by the addition of 1 M NH_3 solution. The stoichiometric amount of $SnCl_2$ (and $AlCl_3 \cdot nH_2O$) was then added with continuous stirring to the solution previously heated to 80 °C. The resulting solution was dried by continuous heating inside a fume box, while the pH was controlled with NH_3 additions. The final stoichiometries were Al/(Al + Sn) = 0 and Sn:Cit = 1:2, 1:3 samples henceforth referred to as Sn-20 and Sn-30, respectively, and Al/(Al + Sn) = 0.1 and (Sn + Al):Cit = 1:2, 1:3 referred to as Al-20 and Al-30.

The thermal decomposition of the precursors to obtain the tin oxide products was carried out after complete drying. The solid residues were heated to 450 °C in air with a heating rate of 5°/min and then annealed at this temperature for 24 h under a static air atmosphere: ex-citrate samples Sn-21, Sn-31, Al-21, and Al-31. This treatment was repeated four times to follow the evolution of samples texture and microstructure, leading to samples Sn-24 and Sn-34.

The powder X-ray diffraction (XRD) studies were carried out with a Siemens D5000 apparatus, using Cu Kα radiation. Rietveld refinements were carried out with the aid of a computer program[15] and line-broadening analysis was performed by profile fitting to pseudo-Voigt functions. Transmission electron microscopy (TEM) analyses were carried out on a JEOL-200CX instrument with 200 kV of accelerating voltage.

FTIR spectra were obtained by using a Bomem spectrometer under transmittance conditions in KBr pellets in the 4000−400-cm^{-1} range. Room temperature ^{13}C and ^{27}Al MAS NMR spectra were recorded on a Bruker ACP-400 spectrometer working at 58.89 and 100.61 MHz resonance frequencies, respectively (9.400 T) and at a 5-kHz spinning rate. The aluminum spectra were referenced to an acidified 1 M solution of $Al(NO_3)_3$.

Mössbauer spectra were measured using a conventional constant acceleration spectrometer. The γ-ray source was ^{119m}Sn in a $BaSnO_3$ matrix used at room temperature. To have the same thickness, absorbers were prepared by mixing 20 mg of finely ground samples with Apiezon grease to reach ≈1 mg $^{119}Sn/cm^2$. Cooled samples at 80 and 4 K were studied by using a liquid nitrogen and a liquid helium cryostat. The velocity scale was calibrated by using a ^{57}Co source and metallic iron foil as an absorber. The spectra were fitted to Lorentzian profiles by a least-squares method.[16] The goodness of fit was controlled by χ^2 tests.[17] All isomer shifts reported here are given with respect to the center of a $BaSnO_3$ spectrum obtained with the same source at 293 K.

X-ray absorption (XAS) spectra were collected at the LURE synchrotron facility in Orsay (France) using the synchrotron radiation from the Syn ACO storage ring. The SA22 beam line was equipped with a high-resolution plane-grating monochromator of 0.2-eV resolution for the oxygen 1s edge. The spectra were recorded in electron yield mode in the 500−570-eV range.

Electrochemical experiments were carried out in two-electrode, Swagelok cells of the type: Li/$LiClO_4$ (propyelene carbonate (PC):ethylene carbonate (EC))/SnO_2. Electrodes using oxide samples as active material were prepared as 7-mm-diameter pellets by pressing at 200 MPa a mixture of 80% of the sample (≈12 mg) and 8% of ethylene−propylene−diene monomer (EPDM) copolymer and 12% carbon black (Strem 4N) to improve the mechanical and electronic conduction properties. Lithium electrodes consisted of a clean 7-mm-diameter lithium metal disk. The electrolyte solution (1 M $LiClO_4$ in a 1:1 mixture of bidistilled PC and EC) was supported by porous glass-paper disks. All cell manipulations were carried out inside a glovebox (M. Braun) under an argon atmosphere (water content <2 ppm). The electrochemical measurements were obtained by a multichannel system, MacPile,[18] alternatively working under potentiostatic and galvanostatic conditions. Prior to the potentiostatic experiments, the cells were allowed to relax until the condition dV/dt < 1 mV/h was fulfilled. Step potential electrochemical spectroscopy (SPES) was carried out by using 10-mV steps. Current relaxation was recorded for 1 h at each step.

3. Results and Discussion

3.1. Characterization of the Tin and Tin−Aluminum Citrate Precursors. The pure tin citrates and aluminum-doped precursors with $SnCit \cdot xH_2O$, $SnCit_2 \cdot xH_2O$, $SnCit_3 \cdot xH_2O$, $Al_{0.1}Sn_{0.9}Cit_2 \cdot xH_2O$, and $Al_{0.1}Sn_{0.9}Cit_3 \cdot xH_2O$ nominal compositions that were prepared by heat drying the corresponding aqueous solutions were obtained as white-gray voluminous powders. The citrate compounds present in the sample were X-ray amorphous and were accompanied by significant amounts of crystalline NH_4Cl, which were completely lost upon heating.

The FTIR spectra of the tin citrate precursors and Al-doped derivatives (Figure 1) show two characteristic bands in the 1400−1480- and in the 1590−1650-cm^{-1} wavenumber ranges, which are ascribable to the symmetric, ν_s, and asymmetric, ν_{as}, vibrations of the deprotonated carboxylate group, respectively. Because of the sensitivity of the ν_{as} and ν_s vibrations toward the mode of carboxylate coordination, the spectra may clearly show whether the deprotonated carboxylate groups are monodentate, chelating bidentate, or bridging.[19] The smaller difference between ν_{as} and ν_s frequencies and the higher ν_s frequency for sample Sn-30 is indicative of bridging carboxylate groups, while Al doping increases the contribution of unidentate groups, probably as a result of a change in coordination of Al(III) ions.

In addition, signals at 1680−1730 cm^{-1} are also visible in the spectra of Figure 1, which are ascribable to C═O stretching in carboxylic acid groups. The experimental spectra clearly show a large amount of protonated carboxylate groups, which are indicative of the excess of citric acid molecules in the amorphous

(15) Young, R. A.; Wiles, D. B. *J. Appl. Crystallogr.* **1982**, *15*, 430.
(16) Rubenbauer, K.; Birchall, T. *Hyperfine Interact.* **1979**, *7*, 125.
(17) Gruverman, I. J.; Seidel C. W. *Mössbauer Effect Methodology*; Plenum Press: New York, 1970.
(18) Chabre, Y.; Djurado, D.; Armand, M.; Romanow, W. R.; Coustel, N.; McCauley, J. P.; Fischer, J. E.; Smith; A. B. *J. Am. Chem. Soc.* **1992**, *114*, 764.
(19) Nakamoto, K. *Infrared and Raman Spectra of Inorganic and Coordination Compounds*, 4th ed.; J. Wiley & Sons: New York, 1986; p 232.

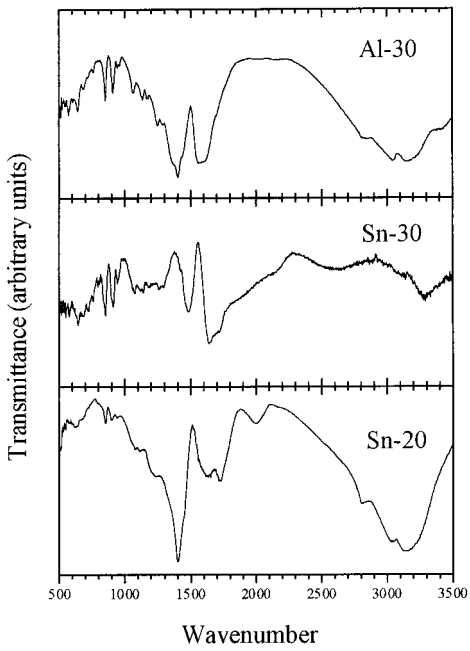

Figure 1. FTIR spectra of citrate precursors of pure and Al-doped tin dioxide.

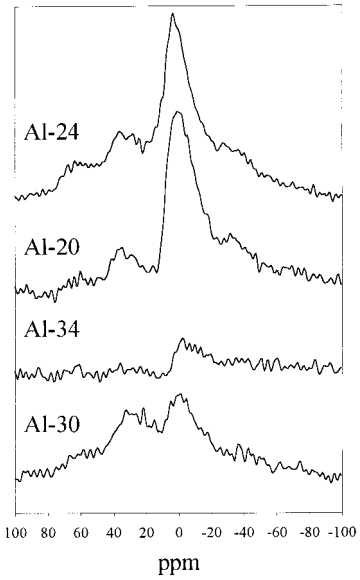

Figure 2. ^{27}Al MAS NMR spectra of precursor and heat-treated samples.

solid, as compared to other stoichiometric compositions, such as those reported in crystalline solids by Deacon et al.[14]

The ^{27}Al MAS NMR spectra of the precursor samples Al-20 and Al-30 (Figure 2) differ in the number of signals: Both samples show a resonance located at ≈0 ppm, while the Al-30 sample shows a second broadened resonance at ≈25 ppm, which overlaps with the spinning sidebands (SSB) of the main signal. According to the liquid-state ^{27}Al NMR spectra of aluminum chloride with citric acid found in the literature, a similar broadened band has been ascribed to the formation of multiligand complexes or to several types of coordination involving changes in the number of chelate rings formed.[20] This result agrees well with the possible changes in aluminum coordination, which modify the FTIR spectra of the precursors as discussed above.

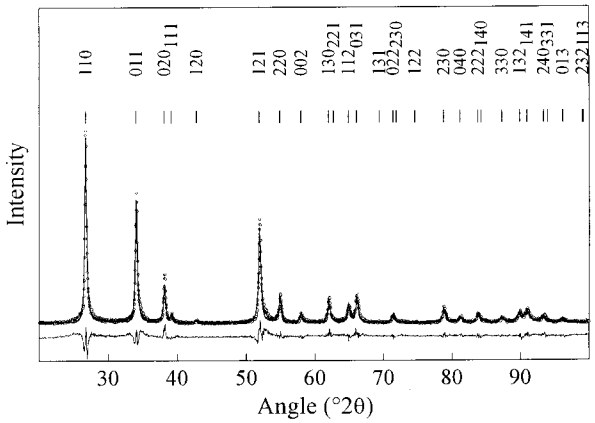

Figure 3. Experimental (open circles), calculated (full line), and difference (below) profiles of XRD data of the Al-31 ex-citrate sample.

3.2. Structural Characterization of the Tin and Tin−Aluminum Oxide Products. The thermal decomposition of the citrate precursors under the experimental conditions used in this study always resulted in the formation of tin-dioxide-related products. The Rietveld refinement of X-ray diffraction data of these products (Figure 3) was carried out by using a rutile-type basic structure to describe the oxide phase ($P4_2/mnm$ space group, Sn in 2a sites and O in 4f sites with $u \approx 0.31$). For Al-containing solids, a random distribution of Al and Sn ions in 2a sites was assumed. The unit cell and broadening parameters evaluated in this analysis are collected in Table 1. The refinement parameters R_{BRAGG} and S are also included and show that the deviations are significant, specially for samples prepared after four heat treatments. This may be a result of local deviations from the stoichiometry generated by the presence of trivalent aluminum and crystallographic shear phenomena, as discussed below in the light of TEM observation.

From the cell parameters in Table 1, little changes in the unit cell dimensions are observed. For samples with a similar heat treatment, the presence of Al involves slightly lower a and c values. This agrees with a random distribution of Al and Sn ions, which should decrease the unit cell dimensions. A similar effect is expected by successive thermal treatments in pure tin samples. Thus, the possible partial reduction in the O/M ratio leading to oxygen vacancies and their elimination process by crystallographic shear should also lead to a slight diminution of a and c parameters, as shown in Table 1.

XRD line-broadening analysis was carried out simultaneously with the Rietveld refinement by profile fitting to pseudo-Voigt functions. The U, V, and W broadening parameters together with the η parameter of the pseudo-Voigt function are included in Table 1. The pseudo-Voigt function is defined as $pV = \eta L + (1 - \eta)G$, where L and G are the Lorentzian and Gaussian contributions to the profiles, which are in turn ascribable to low crystallite size and high microstrain content, respectively. From these results it can be observed that

(20) Thomas, F.; Masion, A.; Bottero, J. Y.; Tekely, P. in *NMR Spectroscopy in Environmental Chemistry*; Nanny, M. A., Minear, R. A., Leenheer, J. A., Eds.; Oxford University Press: Oxford, 1997; p 165.

Table 1. Results of the Rietveld Refinement of Powder X-ray Diffraction Data of Pure and Al-Doped Ex-citrate SnO_2 Samples

sample	*a*/Å	*c*/Å	*u*	*U*	*V*	*W*	η	$S(R_{WP}/R_{EXP})$	R_{BRAGG}
Al-21	4.7402_5	3.1869_4	0.307_3	0.27_4	-0.35_4	0.16_1	0.56_4	1.37	0.0924
Al-24	4.7410_4	3.1872_3	0.300_2	0.13_3	-0.21_3	0.13_1	0.61_3	1.83	0.0866
Al-31	4.7435_3	3.1888_2	0.310_2	0.13_2	-0.17_2	0.10_1	0.46_3	1.20	0.0701
Al-34	4.7430_4	3.1876_3	0.311_3	0.07_2	-0.12_3	0.09_1	0.66_3	1.43	0.1226
Sn-31	4.7442_4	3.1906_3	0.303_2	0.18_3	-0.24_4	0.16_1	0.52_3	1.41	0.0599
Sn-34	4.7416_4	3.1882_4	0.306_3	0.06_3	-0.11_3	0.10_1	0.63_3	1.29	0.0928

for the three ex-citrate samples an increase in η values and a decrease in the angle-independent component *W* of the full width at half-maximum (fwhm = $U \tan^2 \theta + V \tan \theta + W$) are found from one to four thermal treatments. Both effects involve a significant decrease in the content of microstrains upon prolonged thermal treatment.

3.3. Local Environment of Al and Sn Atoms in the Oxide Products. ^{27}Al MAS NMR spectra of the heat-treated samples after four consecutive thermal treatments evidence a single resonance at ≈0 ppm and the corresponding SSB (Figure 2). Although the interpretation of ^{27}Al NMR spectra is complicated by the quadrupolar interaction resulting from the spin $I = 5/2$ and the fact that MAS measurements can only average efficiently first-order broadening effects, the presence of AlO_4 and AlO_6, and more recently, aluminum pentacoordinated by oxygen, is clearly resolved in crystalline and amorphous materials and minerals.[21−27] In these studies, the chemical shift of the ^{27}Al resonances in the 0−8 ppm range are unambiguously accepted to originate from hexacoordinated Al. In the ex-citrate samples, we can identify an octahedral coordination of aluminum in the oxide, which agrees well with the rutile-type structure of SnO_2. Thus, an isomorphic substitution should account for the Al doping, which gives support to the structural model used in the Rietveld refinements.

The main conclusions of TEM observations of the tin oxide particles obtained by the thermal decomposition of the citrate precursors are as follows. For the undoped tin oxide, an average particle size of 50−100 nm was observed. From one to four thermal treatments, the particle size approximately doubles. For Al-doped tin oxide, the particle size is smaller in Al-containing samples and the size homogeneity is poorer, irrespective of the precursor (Cit3 or Cit2). Samples heated four times sinter less than the undoped samples and the sintered particles develop a marked central streak (Figure 4). These effects can be considered as a consequence of the isomorphic substitution of Sn(IV) by Al(III), as shown by ^{27}Al MAS NMR which induces some lattice distortions as the size of the ions differs significantly (0.71 and 0.50 Å, respectively),[28] avoiding large particle sizes. Moreover, forced sintering by successive thermal treatments is achieved by developing zones of lattice relaxation by accumulating two-dimensional defects or eliminating vacancies by crystallographic shear. Recently,[29] it was shown that the main defects in nanosized crystallites of rutile-related SnO_2 are dislocations with [101] Burgers vector and extended dislocations that are composed of a crystallographic shear plane (CSP) oriented parallel to {101} and two partial dislocations of Burgers vector [1/2 0 1/2].

Figure 5 shows the experimental and calculated ^{119}Sn Mössbauer spectra of the ex-citrate oxides. The observed absorption is characteristic of Sn^{4+} in oxygen 6-fold coordination as is observed in pure SnO_2 (isomer shift (IS) = 0, quadrupole splitting (QS) = 0.54 mm/s). The absence of absorption in the range 3−3.5 mm/s excludes the possibility of Sn^{2+} existence. The parameters obtained from the fitting of the profiles to single quadrupole-split Lorentzian lines are shown in Table 2. The hyperfine parameters of the spectra of all samples are similar and very close to those of SnO_2. This can be interpreted by assuming that Al substitution as well as thermal treatments have little effect on the tin local environment. However, there are significant differences in the absorption by the samples. Thus, an increase in absorption is observed from one to four thermal treatments, which is particularly evident in Al-containing oxides, irrespective of the citrate/metal ratio of the precursor (Table 2). This effect is a result of an increase in the percentage of tin atoms that contribute to the Mössbauer effect.

Two alternative explanations can be given to such observation. First, a larger tin content in samples heat treated four times could explain this phenomenon. However, the deviations form SnO_2 stoichiometry that may result, for example, from the formation of crystallographic shear (CS) could not account for the large increase in absorption found for Al-containing samples. A second interpretation could be that the recoil-free fraction of tin atoms increases with the heat treatments. Such an effect can be a consequence of a larger structural rigidity in heat-treated samples due to the loss of internal strains during the heat treatment. This interpretation agrees well with the broadening parameters derived from the Rietveld refinement and discussed above in terms of microstrains release.

Moreover, these results put into evidence a positive effect of Al substitution in SnO_2, which allows a significant improvement of lattice rigidity by heating. Such behavior could have interesting consequences in the sintering behavior of these solids, which is particularly interesting from the point of view of SnO_2-based

(21) Dec, S. F.; Maciel, G. E.; Fitzgerald, J. J. *J. Am. Chem. Soc.* **1990**, *112*, 9069.
(22) Weller, M. T.; Brenchley, M. E.; Apperley, D. C.; Davies, N. A. *Solid State NMR* **1994**, *3*, 103.
(23) Stewart, F. F.; Stebbins, J. F.; Peterson, E. S.; Farnan, Y.; Dunham, S. O.; Adams, E.; Jennings, P. W. *Chem. Mater.* **1995**, *7*, 363.
(24) Chee, K. S.; Cheng, Y. B.; Smith, M. E. *Chem. Mater.* **1995**, *7*, 982.
(25) Lippmaa, E.; Samoson, A.; Mägi, M. *J. Am. Chem. Soc.* **1986**, *108*, 1730.
(26) Smith, M. E.; Steuernagel, S. *Solid State NMR* **1992**, *1*, 175.
(27) Alcántara, R.; Lavela, P.; Tirado, J. L.; Zhecheva, E.; Stoyanova, R. *Inorg. Chem.* **1998**, *37*, 264.
(28) Shannon, R. D. *Acta Crystallogr.* **1976**, *A32*, 751.
(29) Zheng, J. G.; Pan, X. W.; Schweizer, M.; Weimar, U.; Gopel, W.; Ruhle, M. *Philos. Mag. Lett.* **1996**, *73*, 93.

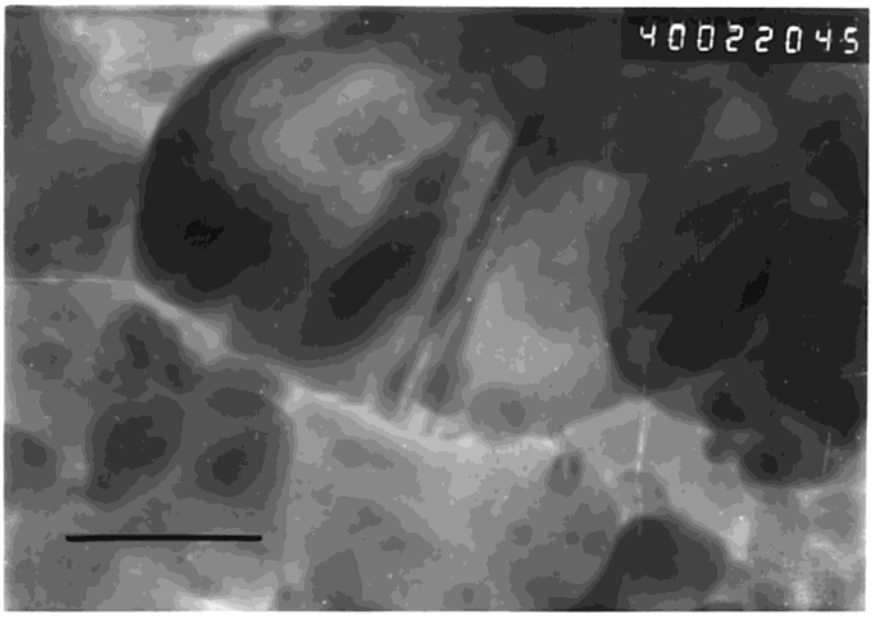

Figure 4. Transmission electron micrograph of ex-citrate tin dioxide Sn-34. Bar = 100 nm.

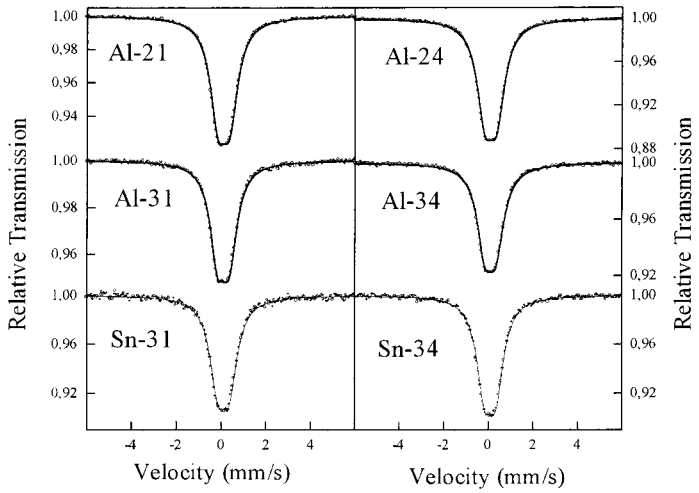

Figure 5. Experimental (circles) and calculated (solid lines) ^{119}Sn Mössbaluer spectra of ex-citrate samples.

Table 2. Isomer Shift (IS), Quadrupole Splitting (QS), Line Width at Half Maximum (LW), and Absorption, Derived from the ^{119}Sn Mössbauer Spectra of Ex-citrate Samples

sample	IS (mm/s)	QS (mm/s)	LW (mm/s)	absorption (%)	Abs(n4)/ Abs(n1)
Al-21	0.007(2)	0.530(3)	0.857(5)	7.77	1.46
Al-24	0.003(1)	0.528(2)	0.873(4)	11.32	
Al-31	0.003(3)	0.526(5)	0.821(8)	5.28	1.50
Al-34	0.008(2)	0.505(4)	0.859(6)	7.91	
Sn-31	0.015(5)	0.515(8)	0.865(13)	9.82	1.02
Sn-34	0.003(3)	0.516(5)	0.837(8)	10.01	

ceramics for ion conductors. The effect of other impurities such as copper[6] or antimony[5] in the sintering and crystallite growth of this oxide have been the subjects of thorough studies in recent years.

While Mössbauer and NMR spectroscopy were used to obtain information about the local environment of tin and aluminum atoms, respectively, a complementary characterization regarding the oxygen anions was obtained by XAS recorded at the O−K edge (Figure 6). Pristine Al-30 and Sn-30 compounds show a well-defined peak at ≈533 eV, followed by a broad band centered at ≈539 eV. After the first heat treatment, the former peak remains in the spectra of sample Sn-31, while the broad band now shows two components at ≈537 and 539 eV. In contrast, sample Al-31 shows the typical profile of SnO_2. After four heat treatments, both samples show the same profile, corresponding to SnO_2. These differences may be related to the different rates of citrate decomposition as discussed below.

To analyze the main features of the XAS spectra of tin, aluminum-doped oxides close to the O−K edge, we first examine a simple model based in a molecular orbital (MO) approach. Only the states more directly involved, and close to the valence and conduction bands, have been considered. The molecular model[30] is based on the Sn-5s, Sn-5p, and O-2p_σ minimal orbital basis, where 2p_σ is the 2p-type orbital pointing toward the Sn atom. Only the sp$_\sigma$ and pp$_\sigma$ two-center interactions are considered because pp$_\pi$ can be neglected and the O-s states are deep in energy (core-like states).

(30) Lippens, P. E.; Olivier-Fourcade, J.; Jumas, J. C.; Georghiu, A.; Dupont, S.; Sénémaud, C. *Phys. Rev. B* **1997**, *56*, 13054.

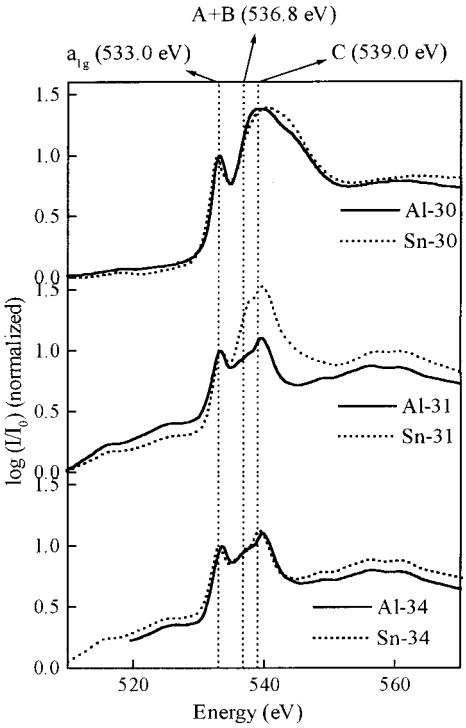

Figure 6. XAS of selected samples.

We first assume that Sn atoms have a perfect octahedral coordination. The obtained MO diagram is illustrated in Figure 7 (left). Three molecular main levels are obtained in the valence band. This simple approach is in good agreement with the experimental high-resolution XPS valence band spectrum, where three peaks are observed.[31] The second band is specially broadened. This fact can be considered as a result of loss of symmetry of SnO_2 as compared with the previous simplified model (O_h), which leads to a splitting of the t_{1u} molecular state.

The XAS spectra at the O−K edge concern transitions between the O-1s state and the empty states of O-p type character. Thus, the main features of the XAS spectra can be compared to the molecular levels with partial O-2p character. Two peaks are predicted by the model, while two bands and a complex shoulder are observed in the experimental K−O edge XAS of SnO_2. To approach the real symmetry around tin atoms in SnO_2, we first distort the octahedron along the *z* axis, changing from O_h to D_{4h}. Then t_{1u} state splits into $a_{2u} + e_u$. Because this distortion is very weak, both states are close in energy, as Figure 7 (right) illustrates. The second distortion modifies the basal planar square into a rectangle, with angles of ≈78° and ≈102°, keeping constant the Sn−O distances. The final symmetry is D_{2h} and t_{1u} is then split in $b_{1u} + b_{2u} + b_{3u}$. Because the precise energetic levels are not known and it is not possible to locate them in the right order, they are indicated as A, B, and C (see Figure 7 (right)), independent of their symmetry, b_{1u}, b_{2u}, and b_{3u}. Thus, the different features in the spectra of Figure 6 can be attributed as follow:

(i) The peak at 533.0 eV corresponds to a transition from the 1s core level of oxygen to a_1 state, due to interactions between the Sn-5s and a combination of O-2p orbitals.

(ii) The peak at 539.0 eV is attributed to a transition to the A state, due to Sn-5p and O-2p interactions.

(iii) The complex shoulder centered at 536.8 eV can be ascribable to transitions to B and C states, also due to 5p-Sn and O-2p interactions.

These attributions are also in agreement with the previous calculation of the partial density of states for SnO_2,[32] where a first peak is observed due to Sn-5s contribution, followed by a complex profile, with Sn-5p contribution. The analysis of the relative intensity and line width of the different bands is complex because the final profile is a convolution of several factors, as the transition probability and the half-life of the electronic core hole and of the excited state. Table 3 collects the energy differences between the various bands observed in our work, as compared to the values in ref 32. Good agreement is observed between both sets of values.

Concerning the products obtained after four heat treatments, no significant differences are observed between samples Sn-34 and Al-34 (see Figure 6), indicating that the presence of Al atoms in the structure does not modify the relative positions of the different antibonding states in SnO_2.

As the first band is clearly defined and has an important 5s(Sn) contribution (spheric symmetry), it can be considered as a "fingerprint" of Sn−O bonds of tin atoms in a pseudo-octahedral coordination, while the splitting of the second band informs of the distortion of the octahedral coordination polyhedron. Thus, because the first band shows no important modifications in the citrate-percursors XAS, it can be assumed that citrate molecules coordinate Sn atoms in a pseudo-octahedral coordination, in agreement with previous published data.[14] The more intense and broadened second band in the citrate XAS as compared with those in oxides can be related to the presence of other atoms bonding oxygen in the citrate ligand (C−O, C═O, O−H bonds). Small differences are observed between the Al-doped and undoped samples, ascribable to the presence of Al atoms coordinated by O.

Marked differences were observed in XAS between Al-containing and pure-Sn samples after the first heat treatment. While in the case of the Al-containing sample, the XAS is close to that obtained after four heat treatments, in the case of the Sn-pure sample, the XAS is intermediate between the citrate percursor and the final product, SnO_2. These results indicate that the decomposition of the 100% Sn citrate compound slowly progresses as compared with the 10% Al citrate sample and that Al somewhat catalyzes the decomposition into an oxide reaction.

Finally, the structures observed below 530 eV (Figure 6) increase in intensity with the number of heat treatments, which seems to indicate that they could be related to SnO_2. They can be tentatively explained as the residual of the M_{IV} and M_V Sn edges, with theoretical energies at 493 and 485 eV, respectively, which

(31) Köver, L.; Kovács, Zs.; Sanjinés, R.; Moretti, G.; Cserny, I.; Margaritondo, G.; Pálinkás, J.; Adachi, H. *Surf. Interface Anal.* **1995**, *23*, 461.

(32) Barbarat, Ph.; Matar, S. F.; Le Blevennec, G. *J. Mater. Chem.* **1997**, *7*, 2547−2550.

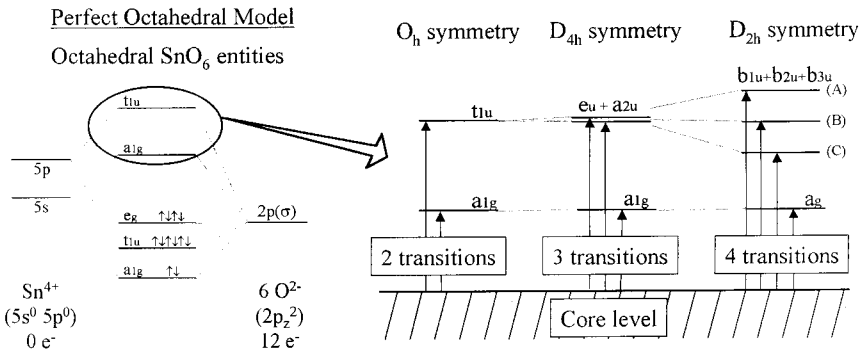

Figure 7. Left: Molecular orbital (MO) approach of SnO_6 polyhedron in an O_h symmetry. Right: Effect of the distortion of a perfecto octahedron according to D_{4h} and D_{2h} symmetries in the splitting of the antibonding states of the MO.

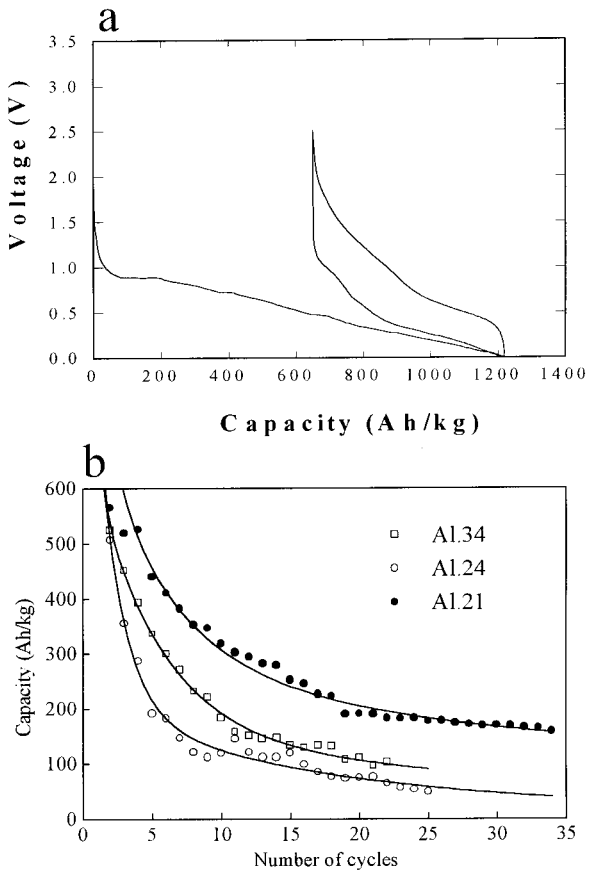

Figure 8. Cycling behavior of lithium cells using the ex-citrate powdered solids as active cathode material. (a) Cell voltage vs capacity for sample Al.21; (b) capacity vs cycle number for selected samples.

becomes more important with the amount of SnO_2 in the samples.

3.4. Electrochemical Study. Figure 8 shows the cycling behavior of lithium anode cells constructed by using the different ex-citrate products as active cathode material. The Li/$LiClO_4$(PC)/sample cells were galvanostatically discharged to 0 V and the upper limit was 2.5 V (see Figure 8a, sample Al21). The total reduction of tin and the formation of lithium−tin alloys accounts for the initial capacity of the cells (≈1220 Ah/kg). However, the reversibility is restricted to the alloying process after complete reduction to tin metal (≈600 Ah/kg of reversible capacity). At this point, a classical description of the reactions of SnO_2[2−4] with lithium explains well the observed behavior. Thus, the reduction of Sn from +4 to 0 would consume 711 Ah/kg and the formation of $Li_{22}Sn_5$, 782 Ah/kg. Even assuming the effect of oxygen atoms in the metal complex,[33] similar discharge capacities have been observed. The reversible capacity decreases markedly after the first cycle up to cycle 15−20 (Figure 8b). After these cycles the capacity stabilizes to a value that depends on the precursor and thermal treatment. The best value of ≈200 Ah/kg is obtained for the bis-ex-citrate product of a single thermal treatment. In comparison, the pure tin compositions showed capacity values well below those of the Al-containing solids. The positive effect of the presence of aluminum is particularly evident after one heat treatment, which is also in correlation with the lower lattice rigidity derived from X-ray and ^{119}Sn Mössbauer measurements.

Table 3. Relative Difference in Energy (in eV) between the Different States in the Valence Band of SnO_2 According to the Molecular Orbital Approach

	a_{1g}	$A + B$	C
a_{1g}	0	3[a]	5[a]
A + B	3.8[b]	0	2[a]
C	6.0[b]	2.2[b]	0

[a] From ref 32. [b] This work.

In conclusion, the facility by which microstrains are released upon successive thermal treatments, specially for Al-containing solids, and the occurrence of CS planes and nonstoichiometry after four heating cycles make necessary strict control of the heating steps in the synthesis of SnO_2 from these precursors, with a view to their application in lithium-ion cells. It should be noted that the values of reversible capacity obtained in our conventional Swagelok cells fall below those reported by Schleich and co-workers[34,35] for thin film SnO_2 electrodes prepared by CVD. These authors reported a reversible capacity of 400−500 mAh/g for 100 cycles. Nevertheless, irrespective of their higher specific capacity, the capacity of thin-film batteries is usually penalized as compared with electrodes with a larger mass of active material. Thus, the use of the materials studied here could be focused to the particular needs of the battery industry.

(33) Chouvin, J.; Olivier-Fourcade, J.; Jumas, J. C.; Simon, B.; Godiveau, O. *Chem. Phys. Lett.* **1999**, *508*, 413.
(34) Brousse, T.; Retoux, R.; Herterich, U.; Schleich, D. M. *J. Electrochem. Soc.* **1998**, *145*, 1.
(35) Retoux, R.; Brousse, T.; Schleich, D. M. *J. Electrochem. Soc.* **1999**, *146*, 2472.

Acknowledgment. The authors express their gratitude for the financial support of the European Commission (Contract ERB-FMBI-98-3020). The authors are grateful to Dr. P. E. Lippens for a critical reading of the molecular model used to analyze XAS data, to J.I. Corredor from Servicio de RMN de la Universidad de Córdoba for his help in obtaining the NMR spectra, and to C. Laffon and Ph. Parent for their help in the X-ray absorption data collection at Lure (Orsay, France). The authors from UCO are also indebted to CICYT (Contract MAT99-0741).

CM991180I